Applied Catalysis B: Environmental 258 (2019) 117982

Contents lists available at ScienceDirect

Applied Catalysis B: Environmental

journal homepage: www.elsevier.com/locate/apcatb

Oxidative dehydrogenation on nanocarbon: Effect of heteroatom doping

Wei Liu[b,1], Chao Wang[a,1], Felix Herold[c], Bastian J.M. Etzold[c], Dangsheng Su[b], Wei Qi[b,d,*]

[a] School of Medical Devices, Shenyang Pharmaceutical University, No. 103, Wenhua Road, Shenyang, 110016, China
[b] Shenyang National Laboratory for Materials Science, Institute of Metal Research, Chinese Academy of Sciences, No. 72, Wenhua road, Shenyang, 110016, China
[c] Ernst-Berl-Institut für Technische und Makromolekulare Chemie, Technische Universität Darmstadt, Darmstadt, 64287, Germany
[d] Department of Chemistry, College of Sciences, Northeastern University, Shenyang, 110819, China

ARTICLE INFO

Keywords:
Oxidative dehydrogenation
Heteroatom doping
Carbon materials
Kinetics
Heterogeneous catalysis

ABSTRACT

Kinetic analysis is a powerful and effective strategy to reveal the physical-chemical nature of the promotion effect of heteroatoms to nanocarbon catalysts. The present work reported the mechanistic and kinetic analysis of ethylbenzene oxidative dehydrogenation (ODH) reactions on heteroatom (N or B) doped and undoped carbon nanotube (CNT) catalysts via active site titration, kinetic isotope effect and single reactant surface reaction experiments etc. The physical-chemical meanings behind the elementary step rate and equilibrium constants were revealed and applied for interpretations of the promotion effect of heteroatoms at molecular level. Nitrogen doped CNT exhibited both higher rate and equilibrium constants for C–H bond dissociation and O_2 adsorption than undoped one via facilitating the electron transfer process. The evolution of the active sites could be quantitatively described with rate equation via the theory of most abundant surface intermediates, which provides in depth understandings on the mechanism and structure-function relations in carbon catalyzed redox reactions.

1. Introduction

Nanocarbon materials have shown great potential as replacements or alternatives for conventional metal based catalysts to meet the urgent demanding of green and sustainable development from modern society considering their relatively high activity, easy availability, low cost and sustainability [1–4]. Carbon catalysis has attracted enormous research interests in the field of catalysis, chemical engineering and material science [5–8]. Comparing with traditional metal based catalysts, nanocarbon materials exhibit advantages of tunable surface chemical composition and structure, providing the possibility for accurate regulation or enhancement of their catalytic activity [3,9,10]. Numerous surface or bulk modification strategies have been developed to synthesize modified nanocarbon with improved catalytic activity [11], and heteroatom doping method has been proved as the most effective one among them [12–16]. It is generally accepted that heteroatoms (such as nitrogen or boron etc.) doped into the graphene lattice would break the conjugation system and influence the electronic structure (namely the redox property) of nanocarbon [17,18]. For example, it has been reported in early research works that nitrogen or boron doped nanocarbon materials exhibit outstanding catalytic activity and great potential in practical applications in alkane (such as ethylbenzene (EB) and n-butane etc.) oxidative dehydrogenation (ODH), electro-catalytic oxygen reduction reaction (ORR) and other energy conversion or storage related reactions [19,20]. However, the synthesis and catalytic applications of doped nanocarbon materials normally rely on typical “trial and error mechanisms”, and one major challenge is the fundamental understandings on the nature of the promotion effect caused by heteroatoms, and which has become a very hot research topic in related fields [21–23].

In the pioneered research work by Dai et al., the promotion effect of nitrogen species on the ORR catalytic activity was proposed [21], and later on it was further revealed by Nakamura and Yao et al. that pyridinic nitrogen species and pentagon defects played a key role in enhancing the ORR activity of carbon via model catalyst systems [22,23]. However these research strategies normally rely on the very special surface engineering techniques or micro-electrochemical characterization methods, which could not be directly applied in heterogeneous catalysis, such as alkane ODH reactions. The fundamental understandings on the promotion effect of heteroatoms on ODH catalytic activity still stayed at its first stage of comparisons of apparent catalytic activity, such as reactant conversion, product selectivity or activation

* Corresponding author at: Shenyang National Laboratory for Materials Science, Institute of Metal Research, Chinese Academy of Sciences, No. 72, Wenhua road, Shenyang, 110016, China.
E-mail address: wqi@imr.ac.cn (W. Qi).
[1] These authors contributed equally to this work.

https://doi.org/10.1016/j.apcatb.2019.117982
Received 14 May 2019; Received in revised form 15 July 2019; Accepted 20 July 2019
Available online 24 July 2019
0926-3373/

energy etc. [19,21], and the lack of in depth physical-chemical interpretations on the nature of promotion mechanism and basic structure-function relations significantly inhibited the further applications and development of heteroatom doped nanocarbon in heterogeneous catalysis.

The present work demonstrated that kinetic analysis is a powerful and effective method to reveal the nature of the promotion effect of heteroatoms on the redox catalytic activity of nanocarbon materials in heterogeneous reactions. We reported the full scale kinetic analysis of EB ODH reactions on N or B doped and undoped nanocarbon catalysts based on active site quantification and turnover frequency (TOF) measurements. The catalytic mechanism is revealed at molecular level through kinetic analysis and temperature programmed surface reactions, and the intrinsic catalytic activity of nanocarbon could be reflected by the rate or equilibrium constants for elementary steps. Heteroatom doping does not always lead to positive effect to the catalytic activity of nanocarbons, and the kinetic model provided detailed guidance for the proper reaction condition selection. The evolution of the active sites on nanocarbon materials during the catalytic process could be quantitatively described by the rate equation, and it also explained the physical-chemical nature of the activity promotion effect from heteroatom doping. The present work provided a feasible kinetic analysis method for the objective evaluations and fair comparisons of the intrinsic catalytic activity of nanocarbon materials, and it also built a basic structure-function relation theory for heteroatom doped nanocarbon catalyzed ODH reactions, which shed light on the rational design and potential applications of this green and sustainable reaction system.

2. Experimental

2.1. Preparation of NCNT

Pristine NCNTs (pNCNT) were synthesized according to reported methods [24]. Catalysts (100 mg) composed of a mixture of Fe, Al, and Mo alloy nanoparticles were heated to 900 °C in a tube furnace. Imidazole (5 g) was heated to 250 °C in a separate tube furnace connected to that with the catalysts. NH_3 (10%) in Ar was subsequently introduced into the linked furnaces from the imidazole side at a flow rate of 100 mL/min. The two furnaces were cooled to room temperature (RT) after 15 min, and the obtained raw products were dispersed in concentrated HCl (50 m L − HCl g-product^{-1}) under vigorous stirring for 6 h at RT. The pNCNT products were collected by filtration and then washed with H_2O until the pH of the filtrate reached 7, and the products were dried at 150 °C. pNCNT was then collected and refluxed in 100 mL HNO_3 (68%) at 120 °C for 2 h. The resulting oxidized pNCNT is labeled as NCNT. The sample was filtered and washed with deionized water until the pH of the filtrate reached 7. Finally, NCNT was dried at 120 °C overnight and collected for further activity tests or characterizations.

2.2. Preparation of BCNT

Pristine BCNTs (pBCNT) were synthesized according to a reported method [25]. 150 mg ammonium pentaborate (CAS: 12007-89-5) and 100 mg CNT was manually mixed. The mixture was heated to 100 °C for 4 h under Ar atmosphere in a tube furnace to remove the adsorbed H_2O, and then it was further annealed at 1500 °C for 30 min with a heating rate of 5 °C/min. The resulted pBCNT sample was then collected and oxidized with refluxing HNO_3 (100 mL, 68%) at 120 °C for 2 h. The obtained oxidized sample, labelled as BCNT, was filtered and washed with deionized water until the pH of the filtrate reached 7. Finally, BCNT was dried at 120 °C overnight and was collected for further activity tests or characterizations.

2.3. Characterizations

SEM images were taken using a FEI Nano450 scanning electron microscope operated at 15 kV. TEM measurements were performed on a FEI Tecnai T12 microscope with an accelerating voltage of 120 kV. The C 1s and O 1s XPS spectra were obtained from a surface analysis system (ESCALAB 250, Thermo VG, USA) with AlKα X-rays (1486.6 eV, 150 W, 50.0 eV pass energy). The XPS spectra were fitted using mixed Gaussian-Lorentzian component profiles after subtraction of Shirley background using XPSPEAK41 software. Raman spectroscopy was performed by a LabRam HR 800 excited with 532 nm laser. The N_2 adsorption/desorption isotherms were collected at −196 °C K using a Micromeritics Tristar 3020 analyzer. The specific surface area was measured by recording N_2 adsorption/desorption isotherms at −196 °C and calculated by the Brunauer-Emmett-Teller (BET) method.

2.4. Ethylbenzene oxidative dehydrogenation reaction activity and chemical titration of active sites

The reaction and titration experimental setup is shown in Fig. S1 [26]. EB ODH reactions on nanocarbon catalysts (CNT, NCNT or BCNT, 100 mg) were performed at 265 °C at ambient pressure using a tubular quartz flow reactor with a plug-flow. The reactant mixture contained EB (99.9%), O_2 (99.999%), and balanced He (99.999%), and the molar flow rates of them were adjusted for the desired EB and O_2 pressures (0.05–16 kPa for EB, 0.25–16 kPa for O_2). The concentrations of reactant and product were measured with gas chromatography (Agilent 7890A) using a methyl silicone capillary column (HP-5, 25 m × 0.32 mm × 1.05 μm) connected to a flame ionization detector and a Porapak Qpacked column (80–100 mesh, 12 ft. × 1/8 in.) connected to a thermal conductivity detector.

In a typical *in situ* titration process, steady state EB ODH rate was firstly measured as introduced above. The syringe for EB inlet was switched to the one containing Phenylhydrazine (PH) (the partial pressure of PH is at around 0.2 kPa) after the reaction reaches steady state (normally after 5 h of the reaction). The reactant, product and the titrant (residual) concentrations were continuously measured by gas chromatography with the same analysis method.

3. Results and discussion

3.1. Chemical structure of undoped and doped CNT catalysts

Undoped carbon nanotube catalysts (CNT) are obtained from the liquid phase oxidation of commercial carbon nanotubes using concentrated nitric acid. The total surface oxygen content of CNT is about 5.7 at.% based on XPS analysis. As deduced from the deconvolution of the O 1s XPS signal (Fig. S2), the major oxygen functionalities on CNT surface are determined to be ketonic carbonyl (O1 species, C═O, 531.5 ± 0.2 eV), carboxylic acid (O2 species, HO−C = O, 532.6 ± 0.2 eV) and hydroxyl groups (O3 species, OH, 533.7 ± 0.3 eV).[27] The C 1s XPS spectrum of CNT exhibits a characteristic sp^2 carbon signal at 284.5 eV (Fig. S3). Raman spectroscopy is an effective method to analyze the structure and defects of nanocarbon materials. The intensity ratio of the D_1 band (1350 cm^{-1}, disordered graphitic lattice) and G band (1580 cm^{-1}, ideal graphitic lattice), denoted by I_D/I_G, is normally used to evaluate the degree of graphitization for carbon materials [27–31]. The clear D_1 band of CNT indicates the existence of defects and edge structures in CNT (Fig. S4), and the measured I_D/I_G value of CNT is at about 1.7. The diameter of CNT catalysts is approx. 20 ± 5 nm as shown in the SEM and TEM images (Fig. S5 and **S6**). The N_2 adsorption result shows that the BET surface area and total pore volume of CNT is 219 m^2 g^{-1} and 1.18 cm^3 g^{-1}, respectively (Fig. S7).

Nitrogen doped carbon nanotube catalysts (NCNT) and Boron doped carbon nanotube catalysts (BCNT) are synthesized using chemical vapor

Table 1
The key structural parameters of CNT, NCNT and BCNT.

Parameters	Catalysts		
	CNT	NCNT	BCNT
Shape	tube	tube	tube
Size (nm)	20 ± 5	50 ± 20	20 ± 5
surface area ($m^2 g^{-1}$)	219	170	255
Total pore volume ($cm^3 g^{-1}$)	1.81	0.45	0.72
I_D/I_G	1.7	1.8	1.7
Total oxygen content (at.%)	5.7	7.9	4.5
C = O content (at.%)[a]	1.2	2.4	1.0
C = O content (C = O g^{-1})[b]	1.54×10^{19}	2.29×10^{19}	1.16×10^{19}

[a] measured by XPS.
[b] measured by chemical titration.

deposition (CVD) and calcination post treatment methods, respectively, and the fabrication procedure is strictly based on literature reported methods [24,25]. Both NCNT and BCNT were also oxidized with concentrated nitric acid prior to catalytic reactions. The total oxygen content and relative concentrations for certain oxygen functionalities for NCNT and BCNT could also be measured via XPS, and their values are listed in Table 1. The synthesized NCNT and BCNT catalysts exhibit tubular morphology with nearly homogeneous distribution of N and B heteroatoms as shown in their TEM and EDS elemental mapping images in Fig. S8 and S9. The similarity of the key physical and chemical parameters (surface area and oxygen content etc. as shown in Table 1) for N and B doped and undoped CNT catalysts enables a fair evaluation of the effect of heteroatom doping on redox catalytic activity. Deconvolution of N 1s and B 1s XPS signals provides the identity, quantity as well as the chemical state of these two types of heteroatoms. As shown in Fig. 1a, pyridinic nitrogen (N1, 398.3 ± 0.2 eV), pyrrolic nitrogen (N2, 400 ± 0.1 eV), quaternary nitrogen (N3, 401 ± 0.1 eV) and nitrogen oxides (N4, 403.3 ± 0.1 eV) are four major nitrogen species existing on NCNT catalysts, and the total content of nitrogen reaches 3.0 at.% [32,33]. It has been reported that quaternary nitrogen species have the most pronounced influence on the electronic properties, namely the redox catalytic activity of nanocarbon [19]. In this case, they account for over 58% of all nitrogen species in the synthesized NCNT sample. The content of boron is 0.6 at.% in the BCNT sample, and boron cluster (B1, 186.5 ± 0.1 eV), B_4C (B2, 187.6 ± 0.1 eV), BC_3 (B3, 188.8 ± 0.1 eV), BC_2O (B4, 190.1 ± 0.1 eV), BCO_2 (B5, 191.3 ± 0.1 eV) as well as boron oxide (B6, 192.8 ± 0.1 eV) are recognized as the major chemical states of boron species based on the deconvolution of the B1 s XPS signal (Fig.1b) [34–36]. Different from nitrogen doping, most of the boron atoms are introduced onto nanocarbon as functionalities but not into the graphitic lattice. The signal belonging to BC_3 species (representing B atoms doped into graphitic lattice) are very weak as shown in Fig. 1b, which may weaken the doping influence on catalytic activity, since it has been reported that BC_3 species are responsible for the enhanced activity of boron doped nanocarbon in both liquid and gas phase reactions [4,12,25,34]. In fact, we found that it is very difficult to substitute sp^2 carbon with boron atoms, which is also consistent with theoretical predictions, since B has a larger size than N [37].

3.2. Kinetic measurements and reaction mechanism

The establishment of the kinetic model requires rigorous measurements of the intrinsic catalytic activity (turnover frequency, denoted as TOF) of nanocarbon catalysts. The difficulty in determining TOF for carbon catalysts does not only exist in measuring the reaction rates but also in rigorous quantification of the active sites. Very recently, we have developed an in situ chemical titration method, which has been proven as an effective method that could realize the determination of the TOF value through one single measurement [26]. As shown in Fig. S10, the in situ active site titration process is performed when EB ODH reaction reached steady state. Phenylhydrazine (PH) is chosen as titrant (poison), which would react with ketonic carbonyl groups forming hydrazones with a yield over 99% [26]. As shown in Fig. S10, the ODH reactivity dramatically dropped after introduction of PH because of the removal of ketonic carbonyl groups. The number of active sites could be obtained through the consumption of the titrant determined by GC analysis. Finally, the TOF could be calculated through the linear dependence between the apparent catalytic activity and the consumption of titrants (namely the slope of the line in Fig. S10). The TOF for CNT catalysts in EB ODH reactions is determined at the magnitude of ~10^{-4} molecules-EB C = O^{-1} s^{-1}, which is similar to that from other quantitative methods, such as TPD [38,39], or *ex-situ* titration [29] et al. It should be mentioned that the reaction conditions were chosen very gentle (265 °C) in the kinetic region (EB conversion < 10%, space velocity without the influence of diffusion, as shown in Fig. S**11**), and to ensure that the measured TOF is not influenced by structural instability (both catalysts and titration derivatives) and could reflect the intrinsic catalytic activity of nanocarbon catalysts under the given reaction conditions. CNT catalysts exhibit stable EB ODH activity for over 200 hs

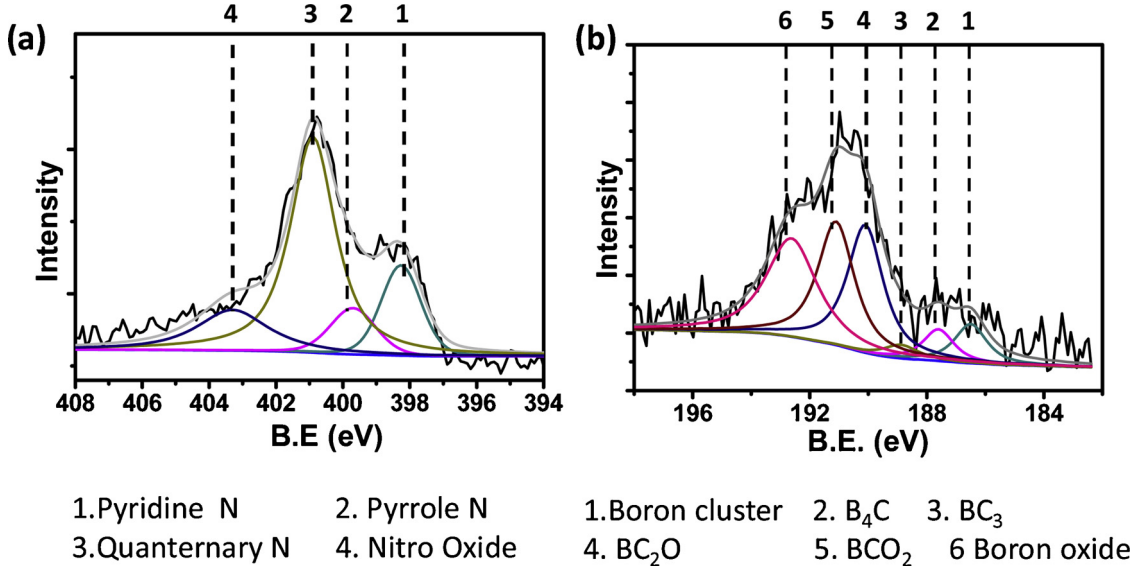

Fig. 1. (a) N 1s XPS spectrum of NCNT. (b) B 1s XPS spectrum of BCNT.

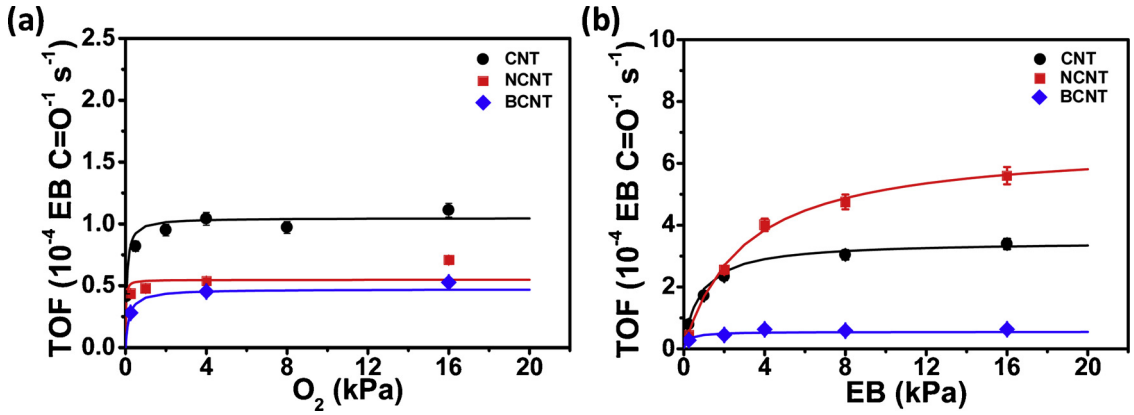

Fig. 2. (a) EB conversion rate (TOF) as a function of O_2 partial pressure for CNT (●), NCNT (■) and BCNT (◆); 265 °C, 0.25 kPa EB. (b) EB conversion rate (TOF) as a function of EB partial pressure for CNT (●), NCNT (■) and BCNT (◆); 265 °C, 16 kPa O_2.

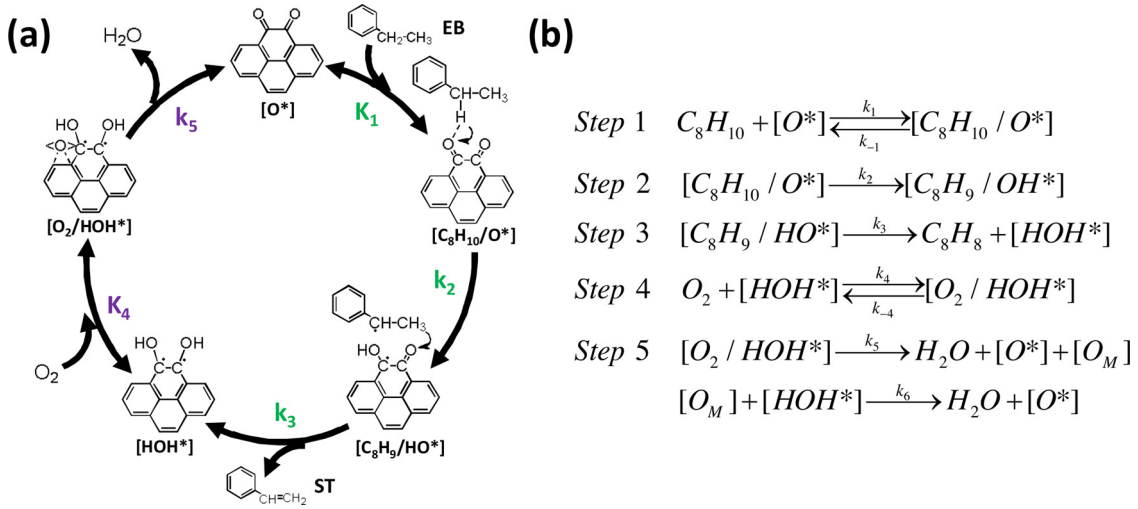

Scheme 1. The proposed reaction pathway (a) and the corresponding elementary steps (b) for EB ODH on nanocarbon catalysts.

under the chosen reaction conditions [4,13]. Raman, XPS and TEM measurements on the recovered catalysts suggest that ODH reaction and subsequent titration process have shown no obvious influence on the skeleton of CNTs (See Fig. S2-S7 in supporting information).

Following the same procedure, we have systematically measured the ODH rates catalyzed by undoped and doped CNT catalysts under different conditions, and the EB conversion rate (TOF) as a function of EB and O_2 partial pressures are shown in Fig. 2. EB ODH rates reach constant value at higher oxygen partial pressure (O_2 partial pressure > 4 kPa), but increase monotonically with the increasing of EB partial pressure (0–16 kPa EB, 16 kPa O_2), indicating that the reaction is kinetically controlled by the activation of EB in a relatively wide range (O_2/EB > 1:64). Kinetic isotopic effects (KIE), defined as the ratio of reaction rates for heavy atom labeled and unlabeled reactants, can also be applied to probe the kinetic relevance of elementary steps, and it verified above kinetic observations. The reaction rate ratio between unlabeled and deuterated EB ($R_{EB}/R_{D\text{-}EB}$) reaches ~2.4 even in reaction mixtures containing EB in large excess (2.0 kPa EB and 0.25 kPa O_2) [40]. On the contrary, the KIE value for unlabeled ($^{16}O_2$) and labeled ($^{18}O_2$) O_2 is ~1.0 under the same reaction conditions [40]. The isotopic tracer studies suggest that the activation of O_2 on carbon is easier than that of EB, and C–H bond activation is the kinetically relevant step under commonly chosen ODH reaction conditions (EB/O_2 at around 2), which is consistent with kinetic measurement results.

The reactions (or interactions) between reactants and CNT catalysts were revealed via control experiments using individual reactants, which has been proved as reliable indicator for reaction mechanism [41]. As shown in the mass spectroscopy (MS) signal changing after sole introduction of EB onto CNT catalysts (Fig. S**12a** in Supporting Information), styrene (ST) was immediately formed after EB reacted with CNT catalysts, indicating that the oxidation of EB and formation of ST do not need the assistance of oxygen, similar to alkane ODH reactions on transition metal oxide catalysts, characterized by the typical Mars–van–Krevelen (M–v–K) mechanism. The decrease of ST formation after reaching a maximum symbolizes the full reduction of the nanocarbon catalyst, namely the total transformation of the active sites from ketonic carbonyl groups to hydroxyl groups [41]. The introduction of EB was cut after the CNT catalysts got fully reduced, and isotopic oxygen ($^{18}O_2$) was then introduced [41]. As shown in Fig. S**12b** (in Supporting Information), H_2O forms simultaneously with the introduction of O_2, indicating that the re-oxidation may be a very fast process, which is consistent with KIE experiment results. The formation of $H_2{}^{16}O$ (m/e = 18) and $H_2{}^{18}O$ (m/e = 20) proceeds at nearly the same intensity, indicating that a rapid dissociative chemisorption and exchange of the gas phase oxygen (^{18}O) with surface oxygen (^{16}O) may exist at the initial stage of re-oxidation. [5] The saturated consumption of O_2 and the maximum formation of H_2O indicates the full re-oxidation of the nanocarbon catalyst, finishing one catalytic cycle.

Combining kinetic measurements, KIE experiments and surface reaction results, a detailed catalytic reaction mechanism for the nanocarbon catalyzed EB ODH is proposed as shown in Scheme. 1 [40,41]. There are five steps in one catalytic cycle, including: 1, the dissociative

chemical adsorption of EB; 2, the sequent hydrogen abstraction from EB (reduction of catalyst); 3, the formation and desorption of ST; 4, the dissociative adsorption of oxygen; 5, the sequent re-oxidation of the active sites (formation of H_2O). The proposed reaction mechanism is similar to that firstly found on carbon deposited on oxide catalysts via the redox cycle of quinone-hydroquinone groups [42,43]. This reaction process is similar to Mars-van Krevelen mechanism but happens only on catalyst surface without the participation of lattice oxygen. We assumed that step 1 and step 4 are quasi-equilibrated, and step 2, step 3 and step 5 are irreversible processes, so the corresponding ODH rate equation (Eq. 1) is derived based on pseudo-steady-state hypothesis (PSSH). K_1 and K_4 are the adsorption equilibrium constants for EB (C_8H_{10}) and O_2. k_2, k_3 and k_5 represent the rate constants for the sequential H-abstraction and the re-oxidation of the catalyst, respectively. [C═O] is the quantity of ketonic carbonyl groups determined by the chemical titration process, which is taken as a proxy for the number of accessible redox active sites. The terms in the denominator of Eq. 1 reflect the relative concentration of surface intermediates at redox active sites, which is directly influenced by the operation parameters.

$$\frac{r_{ODH}}{[C=O]} = \frac{k_2K_1}{\frac{1}{P_{C_8H_{10}}} + K_1 + \frac{k_2K_1}{k_3} + \frac{k_2K_1}{k_5K_4}\frac{1}{P_{O_2}} + \frac{k_2K_1}{k_5}} \quad (1)$$

The kinetic model fits well to all selected undoped (CNT) and doped (NCNT and BCNT) CNT catalysts as indicated by the consistency between the simulated and experimental ODH rates as shown in Fig. 3. The relatively high fitting degree (R-square at 0.99) of all the samples suggests that nitrogen and boron doping are not changing the major reaction pathway drastically but moderately maybe in some structural configuration of intermediates or transient states, which is also proved by independent theoretical calculation results [12]. The fitting of the rate equation (Eq. 1) to experimental data yields the rate or equilibrium constants for given steps (Table 2). These kinetic and thermodynamic parameters reflect the intrinsic catalytic activity and are applied to evaluate the effects of heteroatom doping for nanocarbon catalysts.

3.3. Effect of heteroatom doping on the ODH activity of nanocarbon

The rate or equilibrium constants for doped or undoped CNT catalysts have their specific physical chemical meanings that reflect the intrinsic chemical reactivity of the catalysts. For example, k_2 exhibits the catalytic activity of nanocarbon for breaking the first C–H bond, reflecting the free energy differences between transition states for H-abstraction and gaseous EB molecules (and one active site (O*)). It is a perfect scale bar for evaluating the ODH catalytic activity of nanocarbon, since the C–H activation (breaking of the bond) has been

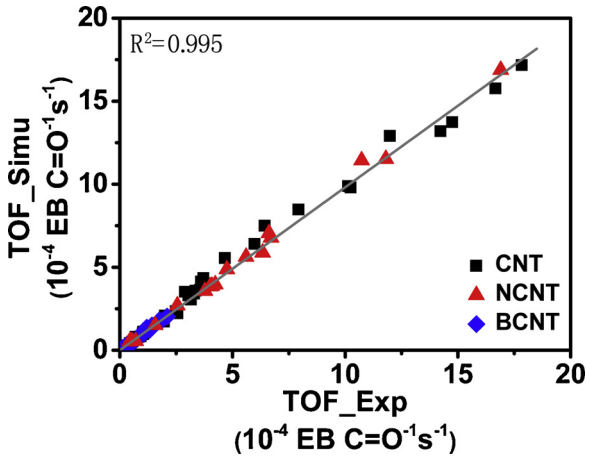

Fig. 3. Correlation between calculated EB TOF and experimentally measured rate data on CNT, NCNT and BCNT samples.

Table 2
The rate or equilibrium constants for CNT, NCNT and BCNT.

rate/equilibrium constant	CNT	NCNT	BCNT
K_1 (kPa^{-1})	2.57×10^{-2}	5.57×10^{-3}	1.84×10^{-1}
k_2 (10^{-2} EB C = $O^{-1}s^{-1}$)	172	408	13.4
k_3 (10^{-2} EB C = $O^{-1}s^{-1}$)	61.6	76.8	5.12
K_4 (kPa^{-1})	0.254	0.477	0.51
k_5 (10^{-2} EB C = $O^{-1}s^{-1}$)	62.9	69.7	5.72

proved as rate determining step (RDS) under common reaction conditions via both experimental (such as KIE) and theoretical calculation results. As shown in Table 2, NCNT exhibits a higher k_2 value than CNT, indicating that the substitution of C with N atoms would increase the C–H bond activation ability of nanocarbon. This observation is consistent with DFT calculation results, which suggest that introduction of nitrogen atoms can increase the spin density on the oxygen atoms in the ketonic carbonyl groups and introduce additional single occupied molecule orbitals, which facilitate the electron transfer between the alkane reactants and the nanocarbon catalysts enhancing C–H bond activation [12,14]. K_4 represents the equilibrium constant for the dissociative adsorption of oxygen molecules on nanocarbon catalysts. The value of K_4 for NCNT catalysts is also higher than that of CNTs, indicating that doping of nitrogen could also facilitate the oxygen activation process. This phenomenon is consistent with electro-catalysis results that doping of nitrogen into the graphitic lattice of nanocarbon could promote the oxygen reduction reactivity [21]. DFT calculation results summarize the nature on promotion of nitrogen doping demonstrating that nitrogen can causes a large decrease in the adsorption energy, alleviating the ability of the catalyst to accept electrons and decrease the energy barrier of alkane dissociation [4,12,14]. In contrast to NCNT, all the rate constants (k_2, k_3 and k_5) for BCNT are slightly lower than those for CNT catalysts. The possible reason for this observation may be due to the absence of BC_3 structure in the synthesized BCNT (no boron atoms were incorporated into the graphitic lattice), but rather the incorporation of surface boron species. These, surface modification boron species seem not to increase the ODH catalytic activity of nanocarbon. Probably these species may slightly influence the adsorption step of EB but show no obvious effect on the redox catalytic ability of nanocarbons. Indirectly, this also suggests that only heteroatom doping to the graphitic lattice influences the electronic structure sufficiently to alter the redox reactivity of nanocarbon materials. Subsequently, we will focus mainly on NCNT samples to show the effect of heteroatom doping in graphitic lattices.

It needs to be pointed out that the description and comparison of intrinsic activities by the rate (k_2) and equilibrium (K_4) constants reflects the fact that NCNT exhibits an enhanced redox catalytic activity compared to undoped CNT catalysts. However, the apparent catalytic activity of the catalysts also depends on the nature of their surface active sites (quantity and oxidation state etc.), which is controlled by the reaction conditions (temperature or the partial pressure of EB and O_2 etc.). The proposed rate equation (Eq. 1) could accurately predict the intrinsic catalytic activity of nanocarbon catalysts, and it helped us to compare different catalysts fairly and also enabled the proper choice of reaction conditions. Fig. 4 summarizes the comparison results of the catalytic activity between NCNT and CNT catalysts with various EB (x axis) and O_2 (y axis) partial pressures. The blue area labeled as “CNT” represents the region where CNT catalysts exhibit higher intrinsic activity (EB ODH rates) than NCNT. Similarly, the pink “NCNT zone” means that the catalytic activity of NCNT catalysts is higher than CNT under these conditions. The gray “spilled zone”, where the sum of EB and O_2 partial pressure exceeds 100 kPa, represents the reaction conditions beyond realization, since the catalytic reaction is performed under ambient pressure. It is clear that the area of the NCNT dominated zone (area in pink) is larger than the corresponding CNT dominated one (area in blue), indicating that NCNT exhibit higher activity under most

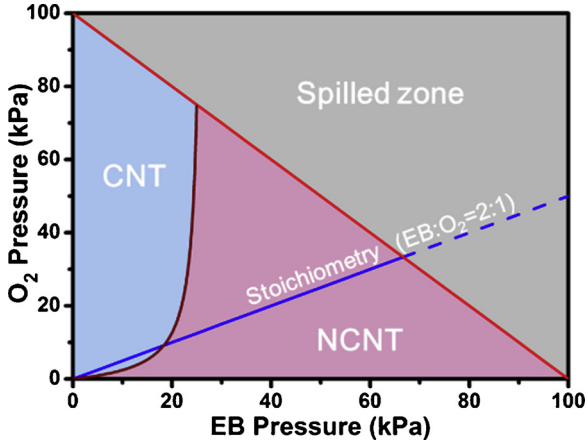

Fig. 4. The overall comparison of the catalytic activity between CNT and NCNT catalysts based on kinetic simulations.

conditions, especially at reaction stoichiometry (the line shown in Fig. 4, EB: O_2 = 2:1). We think this also explains why most of the reported work showed the superiority of nitrogen doping in alkane ODH reactions, because this stoichiometry (EB: O_2 = 2:1) is commonly chosen. However, our analysis in this part revealed that nitrogen doping could not always show positive effects on the ODH catalytic activity of nanocarbon. The detailed kinetic analysis is the basis for the truly fair comparison of different reaction systems, and it is also an important guidance for the proper choice of the reaction conditions to demonstrate the unique advantages of the given catalyst.

The proposed kinetic model enables a quantitative description on the evolution of the active sites on nanocarbons and a comprehensive understanding of the varying of the rate determining step (RDS), which explains thoroughly the difference in catalytic performance among catalysts at molecular level. As indicated by the derivation process, the terms in the denominator of Eq. 1 reflect the relative concentration of each surface intermediate ([O*], [C_8H_{10}/O*], [C_8H_9/HO*], [HOH*], [O_2/HOH*], different forms of active sites), the value of which is influenced by the molar ratio between reactant EB and O_2. The influence of individual steps on the overall reaction rate could be quantitatively explained by the theories of degree of rate control (DRC) [44] or most abundant surface intermediates (MASI), and both of them rely on the analysis of surface intermediates. For example, in the case of CNT, the relative surface concentration of [O*] reaches above 85% at high O_2/EB ratio (O_2/EB > 2). The first term dominates the denominator of Eq. 1, and [O*] is recognized as MASI, namely the abstraction of the first C–H bond of EB is RDS under this reaction condition. Similarly, we could calculate the relative concentration of different surface intermediates under various reaction conditions, and the identity of MASI is plotted as a function of EB and O_2 partial pressure as shown in Fig. 5.

$$\frac{r_{ODH}}{[C=O]} \approx \frac{k_2 K_1}{\frac{1}{P_{C_8H_{10}}}} = k_2 K_1 P_{C_8H_{10}} = k_{1st\cdot ODH} P_{C_8H_{10}} \quad (2)$$

A comprehensive (quantitative) understanding on the catalytic activity difference between CNT and NCNT, namely the promotion effect of N doping, could be achieved via the analysis of MASI (RDS of the reaction). As shown in Fig. 5, both CNT and NCNT share the same MASI ([O*]) at low EB partial pressure (< 2 kPa). The reaction is kinetically controlled by the abstraction of the first H atom from EB. The first term dominates the denominator, and the rate equation could be simplified as Eq. 2, in which $k_{1st,ODH}$ defines a first-order reduction rate constant. $k_{1st,ODH}$ comprises two terms, K_1 and k_2, which means that EB ODH rates are determined by the ability of nanocarbon catalysts in both adsorption and abstraction of H atoms from EB. In case of low EB partial pressures, NCNT exhibits a lower activity than CNT because of its limited adsorption ability of EB even though it exhibits a higher chemical reactivity towards C–H bond breaking (higher k_2). This hypothesis is proved by a control experiment via chemical adsorption of EB on CNT and NCNT catalysts. Fig. 6 shows the desorption profiles of EB that was previously chemically adsorbed on CNT and NCNT (165 °C, 2 kPa EB). It is clear to find that a higher amount of EB desorbed from the surface of CNTs (3.7 times higher signal) than that from NCNTs at a higher desorption temperature (233 °C vs. 219 °C), indicating that CNT exhibits better EB adsorption ability than NCNT in terms of both adsorption capacity and interaction intensity. This observation is in accordance with above kinetic analysis that CNTs have a higher K_1 value than NCNTs.

$$\frac{r_{ODH}}{[C=O]} \approx \frac{k_2 K_1}{\frac{k_2 K_1}{k_5 K_4}\frac{1}{P_{O_2}}} = k_5 K_4 P_{O_2} = k_{O2\cdot ODH} P_{O_2} \quad (3)$$

Following the same analysis procedure, it could be found that the MASI for CNT and NCNT catalysts becomes [HOH*] under "O_2 lean" conditions (O_2 < 0.05 kPa, EB > 3 kPa, the navy blue region in Fig. 5). Dissociative adsorption of O_2 on nanocarbon and the following re-oxidation process (O_2 activation) is the RDS under these conditions. The fourth term dominates the denominator of Eq. 1, and the equation could be simplified as Eq. 3, where $k_{O2\cdot ODH}$ (k_5*K_4) represents the first-order oxidation constant. EB ODH rate depends mainly on the ability of nanocarbon in dissociative adsorption of O_2 and re-oxidation of the catalysts. As shown in Table 1, NCNT exhibit nearly the same k_5 value as CNT catalysts, indicating that once molecular oxygen is dissociated, the formed active oxygen species on these two nanocarbon catalysts exhibit an equal reactivity in re-oxidation of the active sites. The advantage of nitrogen doping is the improvement of the oxygen dissociative adsorption ability of nanocarbon under these reaction conditions, which was also observed in electro-catalysis, such as in ORR processes [21]. For the other regions shown in Fig. 5 (regions around point A and B, respectively) where NCNT also exhibits higher catalytic activity than CNT, the nature of the superiority of nitrogen doping relies on the differences in MASI, namely the shift of the RDS of the reaction. For example, the MASI for CNT and NCNT catalysts are [O*] and [C_8H_9/HO*] at point A (as shown in Fig. 6), and the RDS are the breaking of the first and second C–H bond (abstraction of H atoms), respectively. It is straightforward to understand theoretically and experimentally that the activation of the first C–H bond is more difficult than the second one.

4. Conclusion

In summary, the detailed reaction mechanism and kinetics of doped (N and B) and undoped nanocarbon catalyzed EB ODH processes are proposed via in situ site titration, kinetic, and spectroscopic methods as well as temperature programmed surface reaction. Fair evaluations and comparisons of the intrinsic catalytic activity of doped and undoped CNT catalysts are realized from rate and equilibrium constants. In addition, the proposed kinetic model provides a comprehensive understanding on the effect of heteroatom doping on the redox catalytic activity of nanocarbon. Boron atoms are difficult to introduce into the graphitic lattice of nanocarbon, and the surface modification of nanocarbons with boron species would not alter their intrinsic redox property. Nitrogen heteroatoms could enhance the intrinsic redox property of nanocarbon via promotion of the H abstraction from alkanes and dissociative adsorption of molecular oxygen. The established kinetic model could describe quantitatively the nanocarbon catalyzed alkane ODH reactions and the evolution of the active sites, and predict accurately the catalytic reactivity of the catalysts under different reaction conditions, which provides guidance for proper selections of reaction conditions to exhibit the advantages of heteroatom doped nanocarbon materials. The present research provides a feasible way for quantitatively describing carbon catalyzed ODH reactions under molecular level and fair comparisons of the intrinsic ODH catalytic activity of different

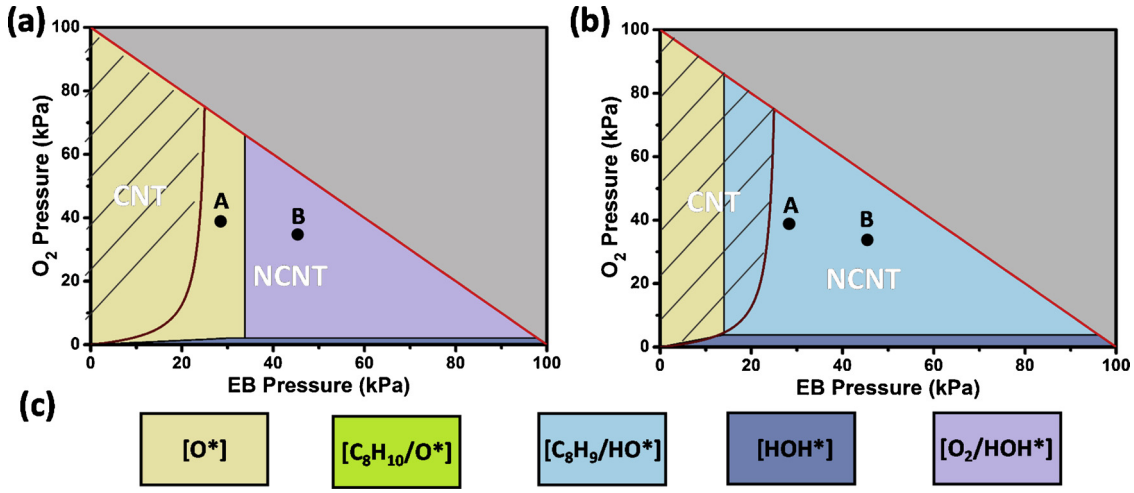

Fig. 5. (a) Most abundant surface intermediates (MASI) distribution of CNT under various EB/O_2 partial pressure. (b) MASI distribution of NCNT under various EB/O_2 partial pressure. (C) The illustration on the identity of MASI.

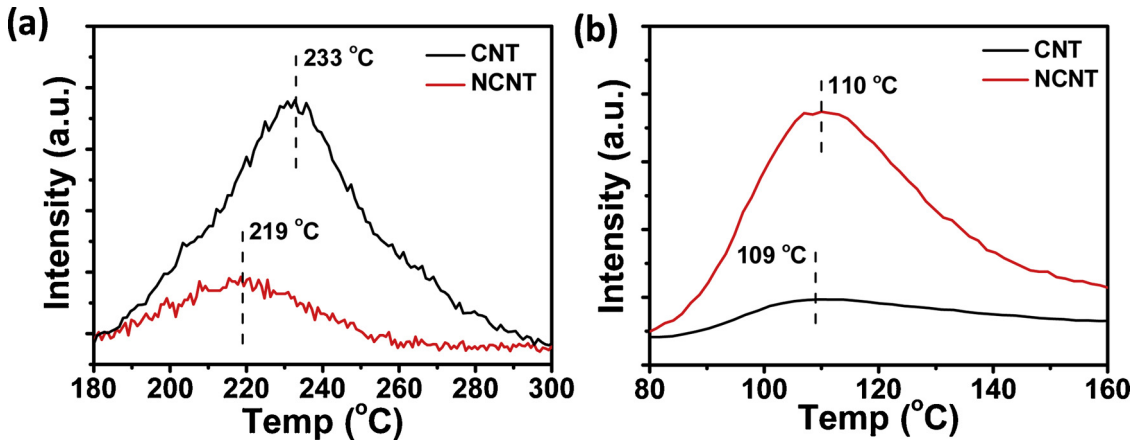

Fig. 6. (a) Mass spectroscopy signal of EB desorption on nanocarbon catalysts (CNT, and NCNT). (b) Mass spectroscopy signal of H_2O during the reaction of O_2 with reduced nanocarbon catalysts (CNT and NCNT).

types of carbon catalysts. It sheds light on the in depth physical-chemical understandings on the effect of heteroatom doping and the establishment of detailed structure-function relationships in the field of non-metallic carbon catalysis, which is the foundation for the rational design of future carbon catalyzed reaction systems.

Declaration of Competing Interest

The authors declare that they have no known competing financial interests or personal relationships that could have appeared to influence the work reported in this paper.

Acknowledgments

The authors acknowledge financial support from the NSFC of China (21761132010, 91645114, and 21573256), and the Youth Innovation Promotion Association, CAS. BE and FH acknowledge the funding of part of the research by the Deutsche Forschungsgemeinschaft (DFG, German Research Foundation) within the project ET-101/13-1. FH acknowledges a fellowship from the Deutsche Bundesstiftung Umwelt (DBU).

Appendix A. Supplementary data

Supplementary material related to this article can be found, in the online version, at doi:https://doi.org/10.1016/j.apcatb.2019.117982.

References

[1] P. Yan, B. Zhang, K. Wu, D.S. Su, W. Qi, Surface chemistry of nanocarbon: characterization strategies from the viewpoint of catalysis and energy conversion, Carbon 143 (2019) 915–936.
[2] J. Zhang, X. Liu, R. Blume, A. Zhang, R. Schlogl, D.S. Su, Surface-modified carbon nanotubes catalyze oxidative dehydrogenation of n-butane, Science 322 (2008) 73–77.
[3] D.S. Su, S. Perathoner, G. Centi, Nanocarbons for the development of advanced catalysts, Chem. Rev. 113 (2013) 5782–5816.
[4] W. Qi, P. Yan, D.S. Su, Oxidative dehydrogenation on nanocarbon: insights into the reaction mechanism and kinetics via in situ experimental methods, Acc. Chem. Res. 51 (2018) 640–648.
[5] W. Qi, D.S. Su, Metal-free carbon catalysts for oxidative dehydrogenation reactions, ACS Catal. 4 (2014) 3212–3218.
[6] J. Zhang, D.S. Su, A. Zhang, D. Wang, R. Schlogl, C. Hebert, Nanocarbon as robust catalyst: mechanistic insight into carbon-mediated catalysis, Angew. Chem. Int. Ed. Engl. 46 (2007) 7319–7323.
[7] P. Yan, Z. Xie, S. Tian, F. Li, D. Wang, D.S. Su, W. Qi, Hydration of phenylacetylene on sulfonated carbon materials: active site and intrinsic catalytic activity, RSC Adv. 8 (2018) 38150–38156.
[8] X. Guo, W. Qi, W. Liu, P. Yan, F. Li, C. Liang, D.S. Su, Oxidative dehydrogenation on nanocarbon: revealing the catalytic mechanism using model catalysts, ACS Catal. 7 (2017) 1424–1427.
[9] R. Schlogl, Carbon in catalysis, J. Adv. Catal. Sci. Technol. 56 (2013) 103–185.
[10] D. Chen, A. Holmen, Z.J. Sui, X.G. Zhou, Carbon mediated catalysis: a review on oxidative dehydrogenation, Chinese J. Catal. 35 (2014) 824–841.
[11] D.S. Su, J. Zhang, B. Frank, A. Thomas, X. Wang, J. Paraknowitsch, R. Schlogl, Metal-free heterogeneous catalysis for sustainable chemistry, ChemSusChem 3 (2010) 169–180.

[12] S.J. Mao, B. Li, D.S. Su, The first principles studies on the reaction pathway of the oxidative dehydrogenation of ethane on the undoped and doped carbon catalyst, J. Mater. Chem. A Mater. Energy Sustain. 2 (2014) 5287–5294.
[13] S. Tian, P. Yan, F. Li, X. Zhang, D.S. Su, W. Qi, Fabrication of polydopamine modified carbon nanotube hybrids and their catalytic activity in ethylbenzene dehydrogenation, ChemCatChem 11 (2019) 2073–2078.
[14] S.J. Mao, X.Y. Sun, B. Li, D.S. Su, Rationale of the effects from Dopants on C-H bond activation for sp2 hybridized nanostructured carbon catalysts, Nanoscale 7 (2015) 16597–16600.
[15] Z.K. Zhao, Y.T. Dai, G.F. Ge, Nitrogen-doped nanotubes-decorated activated carbon-based hybrid nanoarchitecture as a superior catalyst for direct dehydrogenation, Catal. Sci. Technol. 5 (2015) 1548–1557.
[16] Z.K. Zhao, W.Z. Li, Y.T. Dai, G.F. Ge, X.W. Guo, G.R. Wang, Carbon nitride encapsulated nanodiamond hybrid with improved catalytic performance for clean and energy-saving styrene production via direct dehydrogenation of ethylbenzene, ACS Sustain. Chem. Eng. 3 (2015) 3355–3364.
[17] L. Shi, W. Qi, W. Liu, P. Yan, F. Li, J. Sun, D.S. Su, Carbon nitride modified nanocarbon materials as efficient non-metallic catalysts for alkane dehydrogenation, Catal. Today 301 (2018) 48–54.
[18] W. Liu, B. Chen, X. Duan, K. Wu, W. Qi, X. Guo, B. Zhang, D.S. Su, Molybdenum carbide modified nanocarbon catalysts for alkane dehydrogenation reactions, ACS Catal. 7 (2017) 5820–5827.
[19] C.L. Chen, J. Zhang, B.S. Zhang, C.L. Yu, F. Peng, D.S. Su, Revealing the enhanced catalytic activity of nitrogen-doped carbon nanotubes for oxidative dehydrogenation of propane, Chem. Commun. (Camb.) 49 (2013) 8151–8153.
[20] D.S. Su, R. Schlogl, Nanostructured carbon and carbon nanocomposites for electrochemical energy storage applications, ChemSusChem 3 (2010) 136–168.
[21] K. Gong, F. Du, Z. Xia, M. Durstock, L. Dai1, Nitrogen-doped carbon nanotube arrays with high electrocatalytic activity for oxygen reduction, Science 323 (2009) 760–764.
[22] D. Guo, R. Shibuya, C. Akiba, S. Saji, T. Kondo, J. Nakamura, Active sites of nitrogen-doped carbon materials for oxygen reduction reaction clarified using model catalysts, Science 351 (2016) 361–365.
[23] Y. Jia, L. Zhang, L. Zhuang, H. Liu, X. Yan, X. Wang, J. Liu, J. Wang, Y. Zheng, Z. Xiao, E. Taran, J. Chen, D. Yang, Z. Zhu, S. Wang, L. Dai, X. Yao, Identification of active sites for acidic oxygen reduction on carbon catalysts with and without nitrogen doping, Nature Catal. (2019), https://doi.org/10.1038/s41929-019-0297-4.
[24] W. Qi, W. Liu, S.Y. Liu, B.S. Zhang, X.M. Gu, X.L. Guo, D.S. Su, Heteropoly Acid/Carbon nanotube hybrid materials as efficient solid-acid catalysts, Chemcatchem 6 (2014) 2613–2620.
[25] Y.M. Lin, Y.S. Zhu, B.S. Zhang, Y.A. Kim, M. Endo, D.S. Su, Boron-doped onion-like carbon with enriched substitutional boron: the relationship between electronic properties and catalytic performance, J. Mater. Chem. A Mater. Energy Sustain. 3 (2015) 21805–21814.
[26] W. Qi, W. Liu, X. Guo, R. Schlogl, D.S. Su, Oxidative dehydrogenation on nanocarbon: intrinsic catalytic activity and structure–function relationships, Angew. Chem. Int. Ed. Engl. 54 (2015) 13682–13685.
[27] S. Kundu, Y. Wang, W. Xia, M. Muhler, Thermal stability and reducibility of oxygen-containing functional groups on multiwalled carbon nanotube surfaces: a quantitative high-resolution XPS and TPD/TPR study, J. Phys. Chem. C 112 (2008) 16869–16878.
[28] X.Y. Sun, Y.X. Ding, B.S. Zhang, R. Huang, D.S. Su, New insights into the oxidative dehydrogenation of propane on borate-modified nanodiamond, Chem. Commun. (Camb.) 51 (2015) 9145–9148.
[29] W. Qi, W. Liu, B.S. Zhang, X. Gu, X. Guo, D.S. Su, Oxidative dehydrogenation on nanocarbon: identification and quantification of active sites by chemical titration, Angew. Chem. Int. Ed. Engl. 52 (2013) 14224–14228.
[30] A. Cuesta, P. Dhamelincourt, J. Laureyns, A. Martinezalonso, J.M.D. Tascon, Raman Microscope Studies on Carbon Materials, Carbon 32 (1994) 1523–1532.
[31] M.S. Dresselhaus, A. Jorio, M. Hofmann, G. Dresselhaus, R. Saito, Perspectives on carbon nanotubes and graphene raman spectroscopy, Nano Lett. 10 (2010) 751–758.
[32] F.K. Ortega, R. Arrigo, B. Frank, R. Schlogl, A. Trunschke, Acid-base properties of N-Doped carbon nanotubes: a combined temperature-programmed desorption, X-ray photoelectron spectroscopy, and 2-Propanol reaction investigation, Chem. Mater. 19 (2016) 6826–6839.
[33] W. Liu, W. Qi, X. Guo, D.S. Su, Heteropoly Acid/Nitrogen functionalized onion-like carbon hybrid catalyst for ester hydrolysis reactions, Chem. Asian J. 11 (2016) 491–497.
[34] Y.M. Lin, S.C. Wu, W. Shi, B.S. Zhang, J. Wang, Y.A. Kim, M. Endo, D.S. Su, Efficient and highly selective boron-doped carbon materials-catalyzed reduction of Nitroarenes, Chem. Commun. (Camb.) 51 (2015) 13086–13089.
[35] S. Jacques, A. Guette, X. Bourrat, F. Langlais, C. Guimon, C. Labrugere, LPCVD and characterization of boron-containing pyrocarbon materials, Carbon 34 (1996) 1135–1143.
[36] T. Shirasaki, A. Derré, M. Ménétrier, A. Tressaud, S. Flandrois, Synthesis and Characterization of Boron-substituted Carbons, Carbon 38 (2000) 1461–1467.
[37] M. Fyta, Stable boron nitride diamondoids as nanoscale materials, Nanotechnology 25 (2014) 365601–365609.
[38] M. Pereira, J. Orfao, J. Figueiredo, Oxidative dehydrogenation of ethylbenzene on activated carbon catalysts. 1. Inuence of surface chemical groups, Appl. Catal. A: General 184 (1999) 153–160.
[39] M. Pereira, J. Orfao, J. Figueiredo, Oxidative dehydrogenation of ethylbenzene on activated carbon catalysts. 2. Kinetic modelling, Appl. Catal. A: General 196 (2000) 43–54.
[40] W. Liu, C. Wang, D.S. Su, W. Qi, Oxidative dehydrogenation of ethylbenzene on nanocarbon: kinetics and reaction mechanism, J. Catal. 368 (2018) 1–7.
[41] C. Wang, W. Liu, S. Wei, D. Su, W. Qi, Oxidative dehydrogenation on nanocarbon: revealing the reaction mechanism via in situ experimental strategies, ChemCatChem 11 (2019) 397–400.
[42] G. Emig, H. Hofmann, Action of zirconium phosphate as a catalyst for the oxydehydrogenation of ethylbenzene to Styrene, J. Catal. 84 (1983) 15–26.
[43] A. Schraut, G. Emig, H. Hofmann, Kinetic investigations of the oxydehydrogenation of ethylbenzene, J. Catal. 112 (1988) 221–228.
[44] C.T. Campbell, Micro- and Macro-kinetics: Their Relationship in Heterogeneous Catalysis, Top. Catal. 1 (1994) 353–366.